Check for updates

CeO$_2$–Co$_3$O$_4$ nanocomposite with oxidase-like activity for colorimetric detection of ascorbic acid†

Jin Yang, Shiqi Cheng, Shangying Qin, Li Huang, Yuanjin Xu and Yilin Wang ⬤ *

A CeO$_2$–Co$_3$O$_4$ nanocomposite (NC) was prepared and characterized by scanning electron microscopy, transmission electron microscopy, X-ray photoelectron spectroscopy and X-ray diffraction. The obtained CeO$_2$–Co$_3$O$_4$ NC displayed biomimicking oxidase-like activity, which can catalytically oxidize the 3, 3′, 5, 5′-tetramethylbenzidine (TMB) substrate from colorless to the blue oxidized TMB (ox-TMB) product with a characteristic absorption peak at 652 nm. When ascorbic acid (AA) was present, ox-TMB would be reduced, resulting in a lighter blue and lower absorbance. On the basis of these facts, a simple colorimetric method for detection of AA was established with a linear relationship ranging from 1.0 to 500 μM and a detection limit of 0.25 μM. When this method was used to detect AA in human serum and commercially available vitamin C tablet samples, a good recovery of 92.0% to 109.0% was obtained. Besides, the catalytic oxidation mechanism was investigated, and the possible catalytic mechanism of CeO$_2$–Co$_3$O$_4$ NC can be described as follows. TMB is adsorbed on the CeO$_2$–Co$_3$O$_4$ NC surface and provides lone-pair electrons to the CeO$_2$–Co$_3$O$_4$ NC, leading to an increase in electron density of the CeO$_2$–Co$_3$O$_4$ NC. An increased electron density can improve the electron transfer rate between TMB and the oxygen absorbed on its surface to generate O$_2$$^{\bullet-}$ and $^{\bullet}$O$_2$, which further oxidize TMB.

1. Introduction

Ascorbic acid (AA), also known as vitamin C, is one of the essential micronutrients in the human body because of its antioxidant properties. Although AA protects the body from the harmful effects of reactive oxygen and nitrogen species and plays a primary role in preventing cancer, scurvy, and cardiovascular diseases,[1] it cannot be synthesized in the body. AA required by the human body can only be taken from the outside, such as through food or drugs. Therefore, the determination of AA content is very important in disease prevention, food and drug quality assurance. Up to now, various analytical techniques, such as colorimetry,[2,3] fluorescence,[4,5] high-performance liquid phase chromatography,[6,7] capillary electrophoresis,[8,9] electrochemical methods,[10,11] and so on, have been used for AA detection. Because of its fast response, low cost, high sensitivity and good practicability, colorimetry has been preferred. With the development of nanotechnology, various nanomaterials[12–15] have been found to possess peroxidase-like activity. Colorimetry based on the inhibitory effect of AA on peroxidase mimic catalyzed oxidation of 3, 3′, 5, 5′-tetramethylbenzidine (TMB) by H$_2$O$_2$ has been widely used in the determination of AA.[12,13] For example, Ji *et al.*[12] established

a colorimetric method for the detection of AA by employing CoOOH nanoflake as peroxidase mimic. Using Co$_3$O$_4$@CeO$_2$ nanotubes as peroxidase mimic, Lu *et al.*[16] carried out colorimetric determination of AA. Although these methods utilizing peroxidase mimic exhibited high sensitivity, they were limited by the use of unstable H$_2$O$_2$ as an oxidant.

Recent studies have shown that some nanomaterials have oxidase-like activity, which can catalyze the oxidation of TMB by adsorbed oxygen on the material surface or dissolved oxygen in the water. For instance, Co$_3$O$_4$ nanoparticles (NPs) possess oxidase-like activity and can catalytically oxidize TMB in the absence of H$_2$O$_2$. However, the presence of SO$_3$$^{2-}$ can inhibit the Co$_3$O$_4$ NPs-catalyzed TMB oxidation and cause an absorbance decrease. Based on this, a colormetric method for detection of SO$_3$$^{2-}$ was reported by Chen's group.[17] Both SO$_4$$^{2-}$ ion-treated CeO$_2$ nanorods[18] and polyacrylic acid-coated CeO$_2$ NPs[19] exhibit oxidase-like catalytic activity and have been applied for colorimetric detection of glutathione and organophosphorus pesticides respectively. Similarly, Ag NPs-single walled carbon nanotube nanocomposite with oxidase-like activity has been used for the colorimetric detection of AA.[20] Compared with the peroxidase mimic, the oxidation of TMB catalyzed by the oxidase mimic does not use H$_2$O$_2$, which simplifies the determination process.

Although the colorimetric approach based on CeO$_2$–Co$_3$O$_4$ composite as a peroxidase mimic has been used to determine AA[16] and glucose,[21,22] the research on CeO$_2$–Co$_3$O$_4$ composite material as an oxidase mimic has not been reported. In this

College of Chemistry and Chemical Engineering, Guangxi Key Laboratory of Electrochemical Energy Materials, Guangxi University, Nanning 530004, China. E-mail: theanalyst@163.com

work, CeO_2–Co_3O_4 nanocomposite (NC) with oxidase-like activity was prepared by spontaneous precipitation of inorganic precursors. This could provide enough active sites to effectively catalyze the O_2 adsorbed on its surface and accelerate electron transfer in TMB, resulting in the formation of blue oxidized TMB (ox-TMB). As a reductant, AA caused the reduction of ox-TMB, resulting in the blue color fading and absorbance decreasing. Therefore, by measuring the change of absorbance of the CeO_2–Co_3O_4 NC-TMB system before and after adding AA, a colorimetric method for AA detection was established (Scheme 1). It exhibited the advantages of simple material preparation, fast detection speed, high sensitivity, and accuracy.

2. Experimental

2.1 Reagents and instrumentation

Cerium nitrate hexahydrate ($Ce(NO_3)_3 \cdot 6H_2O$), TMB, cobalt nitrate hexahydrate ($Co(NO_3)_2 \cdot 6H_2O$) and glucose were purchased from Shanghai Maclean Biochemical Co., Ltd. Sodium hydroxide (NaOH), sodium carbonate (Na_2CO_3), sodium acetate (NaAc), acetic acid (HAc), ascorbic acid (AA), urea, dopamine (DA) and 2-propanol (IPA) were obtained from Guangdong Guanghua Technology Co., Ltd. p-Benzoquinone (PBQ), glutamine (Gln), serine (Ser), histidine (His), and isoleucine (Ile). Phenylalanine (Phe), lactose (Lac), starch, alanine (Ala), arginine (Arg), glutamic acid (Glu), rhamnose (Rha), fructose (Fru), glycine (Gly), uric acid (UA) and lysine (Lys) were obtained from Tianjin Damao Chemical Reagent Factory.

UV-Vis spectra were obtained from a UV-4802 (Shimadzu, China). The scanning electron microscopy (SEM) images were obtained on a S-3400N microscopy system (Hitachi Co., Japan). Transmission electron microscopy (TEM) images were obtained using a Tecnai G2 F20 S-TWIN (FEI Co., USA). X-ray diffraction (XRD) was determined by a D8 ADVANCE instrument (Bruker AXS Co., Ltd., Germany). X-ray photoelectron spectroscopy (XPS) measurements were implemented with an Escalab 250Xi apparatus (Thermo Fisher Scientific Inc., USA). Electrochemical measurement was carried out on a CHI600D electrochemical workstation (Shanghai, China).

Scheme 1 Schematic illustration of CeO_2–Co_3O_4 NC preparation and AA detection.

2.2 Preparation of CeO_2–Co_3O_4 NC

CeO_2–Co_3O_4 NC with oxidase-like activity was prepared by spontaneous precipitation of inorganic precursors. First, 2.649 g Na_2CO_3 and 100 mL of double deionized water (DDW) were mixed in a 250 mL beaker which was placed in a 60 °C water bath. Then, 5 mL of $Ce(NO_3)_3$ (0.5 M) was slowly added to the beaker with stirring to get a milky turbid solution. After that, 15 mL of $Co(NO_3)_2$ (0.5 M) was added drop by drop to the turbid solution, and the color of the solution gradually changed to taro purple. Followed by adjusting the pH to 10.0 with a NaOH solution of 0.5 M. The reaction continued at this temperature for 5 h, the obtained pink-purple precipitate was transferred to a beaker and washed with DDW several times until the washing solution was neutral. Finally, the washed precipitate was dried at 60 °C for 12 h in a vacuum oven. Before the experiment, 15 mg CeO_2–Co_3O_4 NC was dispersed in 10 mL DDW, and ultrasonic treatment was carried out for 30 min. For comparative study, the pure Co_3O_4 and CeO_2 were also prepared in a similar way.
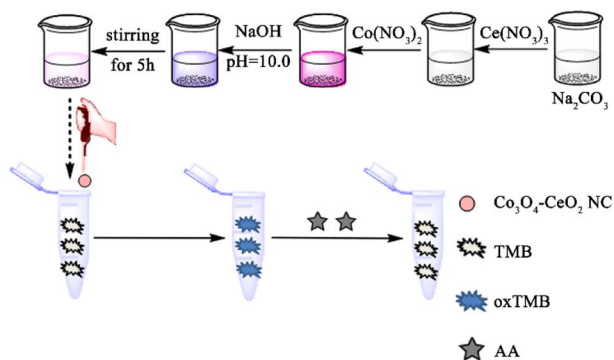
2.3 Procedures for AA determination

In a series of centrifugal tubes, 200 μL of 1.5 mg mL^{-1} CeO_2–Co_3O_4 NC, 200 μL of TMB (10 mM), 1400 μL of HAc-NaAc buffer (pH = 4.0) and 200 μL of AA with different concentration were added in turn. The well-mixed solutions were then incubated at room temperature for 8 min prior to absorption spectra measurement. The decrease of absorbance at 652 nm defined as ΔA ($\Delta A = A_0 - A$, in which A_0 and A represent the absorbance in the absence and presence of AA, respectively) was employed to optimize the detection conditions and establish the calibration curve.

3. Results and discussion

3.1 Characterization of CeO_2–Co_3O_4 NC

The SEM (Fig. 1A) and TEM (Fig. S1†) images indicate that the as-prepared composite is in cluster structure. The HRTEM image (Fig. 1B) shows three lattice spacings of 0.27, 0.31, and 0.29 nm, corresponding to the (200), (111) crystal planes of CeO_2 (ref. 23 and 24) and (220) crystal lattice plane of Co_3O_4,[21,25] respectively. The elemental composition of as-prepared CeO_2–Co_3O_4 NC was obtained by utilizing EDX spectroscopy and displayed in Fig. 1C and D. The presence of O, Co, and Ce in the sample is evident. Moreover, their atomic percentages of them are 73.01, 19.63, and 7.36%, respectively. The atomic ratio of Co and Ce is 2.7 : 1, which is very close to the feeding ratio of 3 : 1. All these confirm that Co_3O_4 nanolayer was successfully grown on the surface of CeO_2 NPs, and the nanocomposite was prepared as expected.

To investigate the crystal structure and chemical composition, the XRD and XPS spectra of CeO_2–Co_3O_4 NC were obtained. As shown in Fig. 2A, the characteristic peaks (2θ) are observed at 19°, 31°, 36°, 38°, 45°, 55° and 59°, corresponding to (111), (220), (311), (222), (400), (422) and (511) crystal planes of the cubic Co_3O_4, respectively, and well-matched with JCPD no. 42-1467. Moreover, the diffraction peaks corresponding to

Fig. 1 (A) SEM and (B) HRTEM images of CeO_2–Co_3O_4 NC, (C) EDX spectrum of CeO_2–Co_3O_4 NC, (D) EDX element mapping images of O, Co, and Ce.

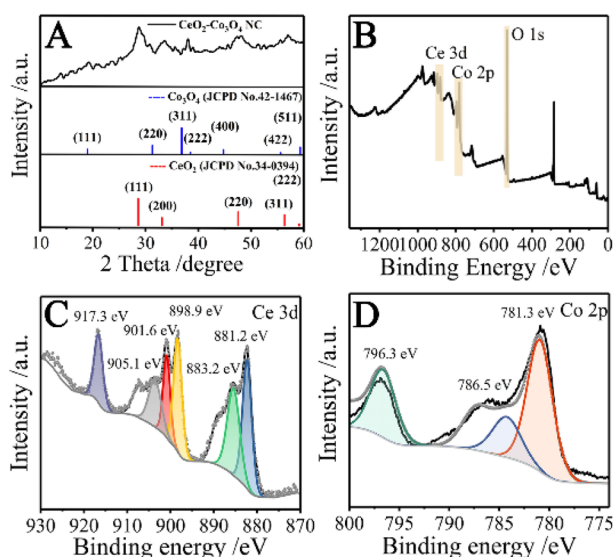**Fig. 2** (A) XRD and (B) XPS spectra of CeO_2–Co_3O_4 NC; (C) XPS of Ce 3d; (D) XPS of Co 2p.

CeO_2 (JCPD No.34-0394), including 28° (111), 33° (200), 47° (220), 56° (311), and 59° (222), can also be observed from the XRD pattern. As can be seen, the obtained CeO_2–Co_3O_4 NC exhibits a weak diffusion peak, indicating the low crystallinity of the sample. Moreover, as seen in Fig. S2A,† both CeO_2 and Co_3O_4 crystalline phases are present in the CeO_2–Co_3O_4 NC, which further confirms the formation of CeO_2–Co_3O_4 NC. Compared with the crystalline phase, low crystallinity possesses rich surface defects and lattice dislocations, which can provide more catalytic sites.[26]

As displayed in Fig. 2B, the existence of Ce, Co, and O elements can be demonstrated in the XPS spectrum of CeO_2–Co_3O_4 NC. To further identify the oxidation state of Ce, the 3d XPS spectrum of Ce was investigated (Fig. 2C). The peaks located at 883.2, 898.9, 901.6, and 917.3 eV are related to Ce^{4+},[26] while the peaks at 881.2 and 905.1 eV correspond to Ce^{3+}.[27,28] These results reveal the existence of mixed valence cerium (Ce^{4+}/Ce^{3+}) in the ceria lattice. The Co 2p spectrum (Fig. 2D) was fitted into three peaks. The peaks at 781.3 and 796.3 eV belong to Co $2p_{3/2}$ and Co $2p_{1/2}$, respectively, indicating the presence of Co^{3+} ions.[29,30] The peak at 786.5 eV can be attributed to $2p_{3/2}$ of Co^{2+} ions.[31] The coexistence of Co^{2+} and Co^{3+} is favorable evidence of the Co_3O_4 phase in CeO_2–Co_3O_4 NC. The spectrum of O 1s (Fig. S2B†) consists of three peaks at 529.9, 531.2 and 532.7 eV, which can be attributed to the lattice oxygen (529.9 eV), defective oxygen (531.2 eV) and chemisorbed oxygen (532.7 eV),[26,29] respectively. The relative content of defective oxygen on the surface of CeO_2–Co_3O_4 NC was calculated to be 38.34%. It should be noted that sufficient surface defects (Ce^{3+}) and high defective oxygen content can improve the catalytic performance of oxidase.[26,32]

3.2 Oxidase-like catalytic activity of CeO_2–Co_3O_4 NC and kinetic analysis

In order to explore the oxidase-like activity of CeO_2–Co_3O_4 NC toward TMB, various chemicals, including H_2O, $Ce(NO_3)_3$, $Co(NO_3)_2$ and CeO_2–Co_3O_4 NC, were mixed with 1600 μL of HAc-NaAc buffer (pH = 4.0, hereinafter referred to as a buffer) containing 200 μL of TMB (10 mM), respectively. Then, the photos of the solution were taken and the corresponding absorption spectra were recorded. As displayed in Fig. 3A, TMB in the buffer is colorless without absorption at 652 nm. TMB in the buffer involving cerium ions and cobalt ions are also colorless, indicating that no oxidation reaction occurs. However, TMB in the buffer containing CeO_2–Co_3O_4 NC results in a blue solution, and strong absorbance at 652 nm is observed, which is similar to MnO_2 NSs,[33] Pd cube@CeO_2 (ref. 34) and Co@N-CNTs[35] catalyzed TMB oxidation. All these results reveal that the obtained CeO_2–Co_3O_4 NC exhibits oxidase-like catalytic activity toward TMB oxidation.

The oxidation of TMB involves electron transfer, and the electron transfer ability of CeO_2–Co_3O_4 NC modified glassy

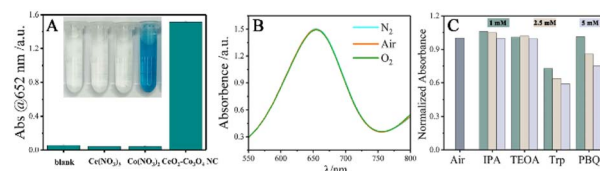**Fig. 3** (A) Absorbance of TMB in different solutions and digital photos of corresponding solutions; (B) absorption spectra of CeO_2–Co_3O_4 NC-TMB systems under air, O_2-saturated and N_2-saturated conditions; (C) control experiment in the oxidation of TMB in the presence of reactive oxygen species scavengers, in which the three colors represent the effect of different concentrations of reactive oxygen scavenger on absorbance (from left to right, the concentration is 1 mM, 2.5 mM, and 5 mM).

carbon electrode (GCE) toward the electrochemical oxidation of TMB was investigated by cyclic voltammetry (CV). The CV responses of TMB at bare GCE and the CeO_2–Co_3O_4 NC-modified GCE are shown in Fig. S3.† Two pairs of well-defined redox peaks of TMB can be observed on all electrodes. Compared with bare GCE, the current of CeO_2–Co_3O_4 NC-modified GCE is significantly enhanced. Suggesting that CeO_2–Co_3O_4 NC shows electrocatalytic activity for the oxidation of TMB and has the ability to promote electron transfer rates between the conductive interlayers.

Generally, the substrate of oxidase mimics-catalyzed TMB oxidation is dissolved oxygen or adsorbed oxygen.[17,36] To identify whether the oxidant for oxidizing TMB was dissolved oxygen or adsorbed oxygen, the CeO_2–Co_3O_4 NC-catalyzed TMB oxidation was first investigated under the conditions of air, N_2, and O_2 saturation, respectively. As shown in Fig. 3B, compared with the air-saturated solution, the activity of CeO_2–Co_3O_4 NC is not inhibited in N_2 saturated solution and not enhanced in O_2 saturated atmosphere, implying that the dissolved oxygen has no effect on TMB oxidation. The O 1s peak at 532.7 eV in the XPS spectrum (Fig. S2B†) reveals the existence of chemisorption oxygen[17] on the surface of CeO_2–Co_3O_4 NC. It has been demonstrated that the chemisorption oxygen on the surface of nanomaterials could lead to the oxidation of TMB.[17] Accordingly, we believe that CeO_2–Co_3O_4 NC catalyzes the chemisorbed oxygen on its surface to oxidize TMB for color development. To identify the reactive oxygen species (ROS) associated with the catalytic reaction, four scavengers, including tryptophan (Trp),[36] *p*-Benzoquinone (PBQ),[37] 2-propanol (IPA),[38] and triethanolamine (TEOA)[39] were used as the quenchers for detecting singlet oxygen ($^\bullet O_2$), superoxide anion ($O_2^{\bullet-}$), hydroxyl radical ($^\bullet OH$), and photogenerated holes (h^+), respectively. As displayed in Fig. 3C, the absorbance of the obtained solution hardly changes with IPA and TEOA scavengers and their concentrations, but decreases with the increase in PBQ and Trp scavenger concentrations. Indicating that the catalytic activity of CeO_2–Co_3O_4 NC is attributed to the generation of $O_2^{\bullet-}$ and $^\bullet O_2$. Based on the above observations, the possible catalytic mechanism of CeO_2–Co_3O_4 NC can be described as follows. TMB is adsorbed on CeO_2–Co_3O_4 NC surface and provides lone-pair electrons to CeO_2–Co_3O_4 NC, leading to an increase in the electron density of CeO_2–Co_3O_4 NC. An increased electron density can improve the electron transfer rate between TMB and the oxygen absorbed on its surface to the generation of $O_2^{\bullet-}$ and $^\bullet O_2$, which further oxidize TMB. Thus, the oxidation rate of TMB by O_2 is accelerated.

To further understand the kinetic mechanism of the oxidase-like activity of CeO_2–Co_3O_4 NC, the apparent kinetic parameters of the catalytic oxidation reaction were measured by varying TMB concentrations. Kinetic parameters were calculated using the double reciprocal of the Michaelis–Menten equation. $1/V = (K_m/V_{max}) \times (1/[S]) + 1/V_{max}$, in which V_{max} and V are the maximal and initial reaction velocity, respectively, [S] refers to the substrate concentration, Michaelis–Menten constant (K_m) indicates the affinity of the enzyme to its substrate. A typical Michaelis–Menten model for CeO_2–Co_3O_4 NC is exhibited in Fig. S4.† The K_m value for CeO_2–Co_3O_4 NC toward TMB was

calculated to be 0.15 mM, which is lower than that of most oxidase mimics (Table S1†), indicating that CeO_2–Co_3O_4 NC possesses a greater catalytic activity toward TMB.

3.3 Application of CeO_2–Co_3O_4 NC in AA detection

Under the catalysis of CeO_2–Co_3O_4 NC, colorless TMB can be oxidized by adsorption oxygen to form blue ox-TMB with an absorption peak at 652 nm. The addition of AA results in color fading and an absorbance decrease. Thus, an analytical method for the colorimetric detection of AA can be established. For the best response, the reaction conditions, including pH, incubation time, and the concentrations of TMB, CeO_2–Co_3O_4 NC, which may affect the change of absorbance, were optimized at room temperature. As illustrated in Fig. S5,† the favourable pH, incubation time, TMB and CeO_2–Co_3O_4 NC concentrations for the CeO_2–Co_3O_4 NC – catalyzed TMB oxidation are 4.0, 8 min, 1.0 mM and 0.15 mg mL^{-1}, respectively. Under the above conditions, the effect of AA concentration on the absorption spectrum of CeO_2–Co_3O_4 NC -TMB system was investigated. As shown in Fig. 4A, the absorbance at 652 nm decreases with the increase of AA concentration. Furthermore, the decrease of absorbance (ΔA) is linear to AA concentration from 1.0 to 500 μM (Fig. 4B) with a regression equation $\Delta A = 0.0016C + 0.0257$ and a correlation coefficient R^2 of 0.9945. A low detection limit of 0.25 μM was obtained based on $3\delta/k$. Compared with existing AA colorimetric detection (Table S2†), this method exhibits a wide linear range and a low detection limit, demonstrating a sensitive method for AA determination.

The selectivity for AA detection was evaluated by using K^+, Mg^{2+}, Ca^{2+}, common sugars (starch, Lac, glucose, Fru, Rha), a series of amino acids (Lys, Phe, Ala, Arg, Glu, Gln, Ser, His, Gly, and Ile), and reducing substances (UA, DA, and urea) as the interferences. The concentration of interfering substances is 20-fold to AA except for UA, DA, and urea which have the same concentration as AA respectively. As shown in Fig. 4C, the ΔA of AA is greater than that of most interferents, implying that the influence of interferents on AA detection can be almost neglected.

To evaluate the feasibility of the method in practical application, the concentration of AA in commercial vitamin C tablets and human serum samples was determined. The vitamin C tablet was purchased from a drugstore in Nanning. A certain quality of tablet powder was dissolved, filtered, and diluted to
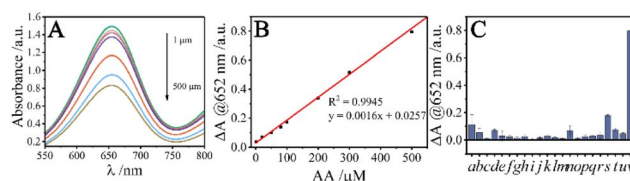

Fig. 4 (A) Absorption spectra of CeO_2–Co_3O_4 NC-TMB in the presence of AA at different concentrations; (B) linear curve formed by fitting ΔA and AA concentration; (C) selectivity of AA assay (From left to right: (a) K^+, (b) Mg^{2+}, (c) Ca^{2+}, (d) starch, (e) glucose, (f) Lac, (g) Fru, (h) Rha, (i) Lys, (j) Phe, (k) Ala, (l) Arg, (m) Glu, (n) Gln, (o) Ser, (p) His, (q) Gly, (r) Ile, (s) UA, (t) DA, (u) urea, and (v) AA).

Table 1 Determination of AA in real samples

Samples	Added (μM)	Measured (μM)	Recovery (%)	RSD (%)
Vitamin C tablet	0.0	311.6	100.5	0.5
	30.0	339.2	97.3	0.6
	50.0	364.5	109.0	2.1
Human serum	30.0	31.7	105.6	3.0
	50.0	46.0	92.0	2.6

prepare the solution to be tested. The serum sample from a healthy adult was provided by volunteer in our team and extracted by Guangxi University Affiliated Hospital (Nanning, China). The serum was 2-fold diluted with BR (pH = 6) buffer. 200 ell of the pre-treated solution was taken, and the detection of AA was performed according to the procedure described in Section 2.3. For standard addition measurement, a certain amount of AA was spiked into the pre-treated sample. As shown in Table 1, the recoveries of AA in two samples are between 92.0% and 109.0%, with the relative standard deviation (RSD) less than 3.0%. The AA concentration was determined to be 311.6 μM in a 110-fold dilution vitamin C tablet sample. Considering the sample weight, the content of AA in vitamin C tablet was calculated to be 92.3 mg g^{-1}, which was consistent with the quantity indicated on the package (91.7 mg g^{-1}). These results demonstrated the CeO$_2$–Co$_3$O$_4$ NC-TMB based colorimetric method is of high accuracy and precision when applied to the measurement of AA in practical samples.

4. Conclusions

We have established a colorimetric method for AA detection based on the oxidase-like activity of CeO$_2$–Co$_3$O$_4$ NC. The proposed method exhibited good selectivity and high sensitivity, which was applied in the determination of AA in actual samples with satisfactory results. The research not only provided a new idea for the construction of nanoenzyme with oxidase-like activity, but also broadened the application range of oxidase mimics. The limitation of the method was that it was not suitable for continuous and *in situ* analysis.

Conflicts of interest

There are no conflicts of interest to declare.

Acknowledgements

Notes and references

1 Y. Guo, J. Du, J. Li, R. Yang, P. d. B. Harrington and Z. Li, *New J. Chem.*, 2021, **45**, 6301–6307.

2 Q. Gao, J. Wan, X. Chen, X. Mo, Y. Sun, J. Zou, J. Nie and Y. Zhang, *RSC Adv.*, 2021, **11**, 39306–39310.

3 X. Shu, Y. Chang, H. Wen, X. Yao and Y. Wang, *RSC Adv.*, 2020, **10**, 14953–14957.

4 K. Xing, J. Ge, W. Wang, X. Geng, X. Shen, J. Tang, L. Qu, Y. Sun and Z. Li, *New J. Chem.*, 2019, **43**, 9466–9471.

5 C. Tang, R. Long, X. Tong, Y. Guo, C. Tong and S. Shi, *Microchem. J.*, 2021, **164**, 106000.

6 N. Baenas, F. J. Salar, R. Domínguez-Perles and C. García-Viguera, *Molecules*, 2019, **24**, 1632–1642.

7 R. Zuo, S. Zhou, Y. Zuo and Y. Deng, *Food Chem.*, 2015, **182**, 242–245.

8 M. M. A. C. Ribeiro, A. A. Prado, A. Domingues Batista, R. Alejandro Abarza Munoz and E. Mathias Richter, *J. Sep. Sci.*, 2019, **42**, 754–759.

9 B. M. C. Costa, A. A. Prado, T. C. Oliveira, L. P. Bressan, R. A. A. Munoz, A. D. Batista, J. A. F. da Silva and E. M. Richter, *Talanta*, 2019, **204**, 353–358.

10 A. Ali, R. Jamal and T. Abdiryim, *RSC Adv.*, 2021, **11**, 33425–33430.

11 S. Cheng, J. Yang, S. Qin, L. Huang, Y. Xu and Y. Wang, *New J. Chem.*, 2023, **47**, 3361–3367.

12 D. Ji, Y. Du, H. Meng, L. Zhang, Z. Huang, Y. Hu, J. Li, F. Yu and Z. Li, *Sens. Actuators, B*, 2018, **256**, 512–519.

13 H. Sun, X. Liu, X. Wang, Q. Han, C. Qi, Y. Li, C. Wang, Y. Chen and R. Yang, *Microchim. Acta*, 2020, **187**, 110.

14 X. Shu, D. Wang, C. Yuan, X. Qin and Y. Wang, *Chem. J. Chin. Univ.*, 2021, **42**, 1761–1767.

15 R. Shi, S. Wei, S. Cheng, J. Zeng, Y. Wang and X. Shu, *Chem. Res. Chin. Univ.*, 2022, **38**, 985–990.

16 Y. Zhu, Z. Yang, L. Song, M. Chi, M. Li, C. Wang and X. Lu, *Part. Part. Syst. Charact.*, 2018, **35**, 1800049.

17 X. Zhang, F. W. Qin, L. Su, C. Yang, Y. Ma, H. Zhang and X. Chen, *J. Agric. Food Chem.*, 2014, **62**, 5827–5834.

18 L. Huang, W. Zhang, K. Chen, W. Zhu, X. Liu, R. Wang, X. Zhang, N. Hu, Y. Suo and J. Wang, *Chem. Eng. J.*, 2017, **330**, 746–752.

19 S. Zhang, S. Xue, J. Deng, M. Zhang, G. Shi and T. Zhou, *Biosens. Bioelectron.*, 2016, **85**, 457–463.

20 F. Li, Y. Yu, F. Xiao, H. Liang, C. Liu, P. Fan and S. Yang, *Luminescence*, 2020, **35**, 1084–1091.

21 D. Jampaiah, T. Srinivasa Reddy, V. E. Coyle, A. Nafady and S. K. Bhargava, *J. Mater. Chem. B*, 2017, **5**, 720–730.

22 N. Alizadeh, A. Salimi and R. Hallaj, *Sens. Actuators, B*, 2019, **288**, 44–52.

23 Y. Lei, W. Li, Q. Liu, Q. Lin, X. Zheng, Q. Huang, S. Guan, X. Wang, C. Wang and F. Li, *Fuel*, 2018, **233**, 10–20.

24 W. Wang, W. Yu, P. Du, H. Xu, Z. Jin, R. Si, C. Ma, S. Shi, C. Jia and C. Yan, *ACS Catal.*, 2017, **7**, 1313–1329.

25 J. Liu, H. Xia, L. Lu and D. Xue, *J. Mater. Chem.*, 2010, **20**, 1506–1510.

26 J. Lian, P. Liu, C. Jin, Q.-Y. Liu, X. Zhang and X. Zhang, *ACS Sustainable Chem. Eng.*, 2020, **8**, 17540–17550.

27 D. Jampaiah, T. Srinivasa Reddy, A. E. Kandjani, P. R. Selvakannan, Y. M. Sabri, V. E. Coyle, R. Shukla and S. K. Bhargava, *J. Mater. Chem. B*, 2016, **4**, 3874–3885.

28 D. Deng, N. Chen, Y. Li, X. Xing, X. Xiao and Y. Wang, *Catal. Lett.*, 2015, **145**, 1344–1350.

29 H. Liu, Y. Ding, B. Yang, Z. Liu, Q. Liu and X. Zhang, *Sens. Actuators, B*, 2018, **271**, 336–345.

30 X. Liu, L. Yan, H. Ren, Y. Cai, C. Liu, L. Zeng, J. Guo and A. Liu, *Biosens. Bioelectron.*, 2020, **165**, 112342.

31 L. Xu, Q. Jiang, Z. Xiao, X. Li, J. Huo, S. Wang and L. Dai, *Angew. Chem., Int. Ed.*, 2016, **55**, 5277–5281.

32 D. Jampaiah, S. J. Ippolito, Y. M. Sabri, J. Tardio, P. R. Selvakannan, A. Nafady, B. M. Reddy and S. K. Bhargava, *Catal. Sci. Technol.*, 2016, **6**, 1792–1803.

33 N. Alam, C. H. Ravikumar, M. Sreeramareddygari, M. Somasundrum and W. Surareungchai, *Anal. Bioanal. Chem.*, 2022, **415**, 703–713.

34 J. Wang, P. Ni, C. Chen, Y. Jiang, C. Zhang, B. Wang, B. Cao and Y. Lu, *Microchim. Acta*, 2020, **187**, 115.

35 T. Chen, J. Cao, X. Bao, Y. Peng, L. Liu and W. Fu, *RSC Adv.*, 2021, **11**, 39966–39977.

36 M. Wang, X. Zhou, S. Wang, X. Xie, Y. Wang and X. Su, *Anal. Chem.*, 2021, **93**, 3130–3137.

37 C. Jin, J. Lian, Y. Gao, K. Guo, K. Wu, L. Gao, X. Zhang, X. Zhang and Q. Liu, *ACS Sustainable Chem. Eng.*, 2019, **7**, 13989–13998.

38 F. Li, N. Li, C. Xue, H. Wang, Q. Chang, H. Liu, J. Yang and S. Hu, *Chem. Eng. J.*, 2020, **382**, 122484.

39 M. Chen, R. Lu and A. Yu, *Mater. Lett.*, 2020, **263**, 127253.